Precision Mass Measurement of ^{9}C, ^{13}O, and ^{21}Mg and the Isobaric-Multiplet Mass Equation*

G. F. Trentelman, B. M. Preedom,† and E. Kashy
Cyclotron Laboratory and Physics Department, Michigan State University, East Lansing, Michigan 48823
(Received 23 February 1971)

The ground-state masses of ^{9}C, ^{13}O, and ^{21}Mg have been determined through measurement of the Q values of the $^{12}C(^{3}He, ^{6}He)^{9}C$, $^{16}O(^{3}He, ^{6}He)^{13}O$, and $^{24}Mg(^{3}He, ^{6}He)^{21}Mg$ reactions. The measurements were made with 68–70-MeV ^{3}He beams using a split-pole magnetic spectrograph. A new method for obtaining a precise calibration for the beam analyzer and magnetic spectrograph at these high bombarding energies is presented.

The mass excess of ^{9}C has been measured as 28.911 ± 0.009 MeV, that of ^{13}O as 23.103 ± 0.014 MeV, and that of ^{21}Mg as 10.912 ± 0.018 MeV. These nuclei represent the $T_z = -\frac{3}{2}$ members of the $T = \frac{3}{2}$ quartets for $A = 9$, 13, and 21, respectively.

The present results show excellent agreement with a quadratic isobaric-multiplet mass equation for $A = 13$ and $A = 21$, but there is some indication that a small cubic term is required for the $A = 9$ multiplet.

I. INTRODUCTION

The isobaric-multiplet concept has been successful in explaining the similar level structure of mirror nuclei and the existence of analog states. Using isospin formalism, it is possible to obtain from first-order perturbation theory an equation quadratic in T_z that relates the masses of members of an isobaric multiplet.[1,2] This isobaric-multiplet mass equation (IMME) can be written as

$$M(\alpha, T, T_z) = a(\alpha, T) + b(\alpha, T)T_z + c(\alpha, T)T_z^2,$$

where M is the mass of a multiplet member, T is the isospin, T_z is the specific isospin projection for the multiplet member, and α represents all of the charge-independent quantities. These charge-independent quantities are assumed to be identical for all members of the multiplet.

Since this equation is quadratic in T_z, one must know the masses of at least an isobaric quartet ($T = \frac{3}{2}$) to test its validity. Such quartets exist but the uncertainties in the mass of the most proton-rich member ($T_z = -\frac{3}{2}$) have made most such tests inconclusive. The most accurately measured $T = \frac{3}{2}$ multiplet ($A = 9$) has shown indications that a term proportional to T_z^3 should be included in the IMME, at least for this quartet.[3-5] The purpose of the work presented here was to accurately measure the masses of other $T_z = -\frac{3}{2}$ nuclei in order to further test the IMME and to see if the need for a T_z^3 term persists. Some of the results of this work have been reported previously.[6]

The experiments described here determined the ground-state masses of the nuclei ^{9}C, ^{13}O, and ^{21}Mg by measuring the Q values of the reactions $^{12}C(^{3}He, ^{6}He)^{9}C$, $^{16}O(^{3}He, ^{6}He)^{13}O$, and $^{24}Mg(^{3}He, ^{6}He)^{21}Mg$. The measurements were made using an Enge-type split-pole magnetic spectrograph.[7] Since the spectrograph can compensate for the kinematic spread of the reaction products, it was possible to use a large detection solid angle. Magnetic analysis of the charged particles also removed the overwhelming background that would be caused by the elastically scattered ^{3}He particles.

II. BEAM SYSTEM AND PARTICLE DETECTION

This experiment used ^{3}He beams from the Michigan State University sector-focused cyclotron. The analysis and transport system[8] was typically set to deliver a beam of maximum energy spread of ±20 keV at 70 MeV and maximum radial divergence of ±2 mrad. The direction of the beam on the target was defined by two sets of current sensitive slits. Continuous monitoring of these slits and the switching magnetic field assured constancy of incident beam direction. Slits defining detection solid angles of 1.2, 0.30, and 0.05 msr were used at the entrance to the spectrograph. For spectrograph calibration runs, the 0.30-msr slit was used, and for the (^{3}He, ^{6}He) reactions the 1.2-msr slit was used. Occasionally a reaction was observed through each of the three slits while the spectrograph field was kept constant. No centroid shift was produced that was significantly greater than the statistical error in the centroid itself.

Particle detection at the spectrograph focal plane was accomplished with a 300-μ-thick position-sensitive silicon surface-barrier detector which subtended 3.0 cm along the focal plane.[9] The energy-loss signals (E) and the position signals (XE) were digitized and used as input to an on-line XDS Sigma-7 computer. The position and identi-

fication of the particles were obtained using the code TOOTSIE[10] which plots the ratio XE/E vs E. This highly flexible code also calculated and displayed the centroids of various particle groups, thus allowing rapid access to the information necessary for the tuning of the various magnets during the calibration procedure. The E and XE signal amplifiers were used in an ac-coupled, doubly differentiated mode. The analog-to-digital-converter zero levels were set to obtain a true zero so that no error in the position signal (XE/E) would arise due to any dc levels. Such dc biases would have given a different XE/E ratio for particles at the same position on the detector if their total energy losses (E) were significantly different, as is the case in the present work for p, d, ^{3}He, and ^{6}He particles. Two different detector geometries were used; the first with particles incident at 45° in which the detector operated in the dE/dx mode, and the second with particles incident at 53° and the detector operating in a stopping mode for the ^{12}C(^{3}He, ^{6}He)^{9}C and ^{16}O(^{3}He, ^{6}He)^{13}O reactions. Rotating the detector 8° relative to the incident particles also increased the effective energy dispersion by about 20%.

It has been observed that the spectrograph magnetic field shape is sensitive to the field-recycling procedure used[11] and to the rate at which the central field is changed. Using a cycling time of 40 min for a field change of 0.0 to 15.3 to 0.0 kG, and taking all data on the cycle with the field always rising to the desired value considerably reduced this effect. Peak locations on separate cycles were repeatable to within the statistical uncertainty of their centroids.

Energy-dispersion matching between the transport system and spectrograph reduced the effects of small beam-energy shifts within the limits set by the beam transport-analysis system. The dispersion-matched condition was created by choosing quadrupole lens settings that gave the dispersed beams a width on target commensurate with that required by the dispersion characteristics of the spectrograph. The degree of dispersion match actually used in these experiments ranged from 50–75% of total match.

To guard against spurious effects on incident beam direction due to stray fields of the cyclotron, bending magnets, the earth's magnetic field, and particularly the spectrograph whose field was often changed, all exposed areas of the beam-transport system were wrapped with soft iron for magnetic shielding.

III. SPECTROGRAPH CALIBRATION AND PARTICLE ORBITS

The spectrograph-field behavior was carefully calibrated between 8.7–13.3 kG with proton beams, and extended to 14.7 kG using ^{3}He beams. The calibration was made for particles in orbits corresponding to an effective radius of curvature (ρ) of about 32.3 in., and all data were taken at a focal-plane position corresponding to this radius. The calibration was accomplished with a momentum-matching procedure developed at this laboratory.[12] The procedure involved the use of proton beams whose energies were determined by simultaneously detecting at the same focal-plane position (corresponding to $\rho \simeq 32.3$ in.) the elastically scattered protons and ground-state deuterons from reactions on ^{12}C. Since the protons and deuterons have different charge-to-mass ratios, their magnetic rigidities were equal for a unique beam energy determined by the ^{12}C(p, d)^{11}C Q value, and the detection scattering angle. For this particular pair of reactions with a ^{12}C(p, d)^{11}C Q value of -16.4953 MeV,[13] a beam energy of 33.691 MeV is required to give the deuterons and elastically scattered protons equal magnetic rigidities when they are detected at 15.0° in the laboratory.

The uncertainties associated with this beam energy came from the uncertainties in the Q value, the scattering angle, and in peak centroid positions. The scattering angle was determined by detecting protons from the ^{1}H(p, p)^{1}H reaction on a very thin Formvar target. Since outgoing proton energies in this reaction are very sensitive to the detection angle, these angles could be measured to a precision of ±0.05° using the beam-energy value given by the transport-analysis system. An uncertainty of ±0.05° in the scattering angle yields an uncertainty of ±1.5 keV in the momentum-matched beam energy.

The difference between proton and deuteron peak centroid positions could be determined to better than 0.1 mm. A 0.1 mm uncertainty in the relative centroid positions would give a beam energy uncertainty of ±1.5 keV. Particle-energy losses in the targets were taken into account and are estimated to have contributed an uncertainty of less than 0.2 keV to the determination of the momentum-matched beam energy. The total uncertainty of the momentum-matched beam energy is therefore estimated to be no more than 1×10^{-4} of the beam energy.

This procedure for determining the beam energy and scattering angle also determined the magnetic rigidity of the scattered protons and deuterons and provided a normalization point for the remainder of the calibration. The value of the radius of curvature corresponding to the focal-plane position, where these and all following reaction products were detected, was defined as the ratio of the proton or deuteron rigidity (they are equal

at the momentum-matched condition) to the spectrograph-field strength measured by the nuclear-magnetic-resonance fluxmeter (NMR). The NMR was located in the flat field region of the spectrograph, between the large pole tips. A collimated ^{241}Am α source was permanently mounted to the focal-plane apparatus below the normal detector position and provided a fiducial mark for the focal-plane position corresponding to this radius. The position on the detector corresponding to the centroid of the α peak marked the required focal-plane position. When amplifier gains were changed to accommodate various particle-energy losses, the detector was lowered to the α source for recalibration.

The remainder of the calibration was accomplished by taking advantage of the precise knowledge of the incident beam energy as determined by the momentum match, and observing reactions whose Q values are well established. The reaction products were detected at the standard focal-plane position. The magnetic rigidities of the resulting reaction products were calculated using the measured beam energy, scattering angle, and kinematic considerations. These calculated rigidities were compared with the empirical rigidities determined using the spectrograph field measured by the NMR and the radius of curvature associated with the standard focal-plane position. Since all reaction products were detected at this position, this comparison of calculated and empirical rigidities provided the required information about the spectrograph-field behavior.

TABLE I. Spectrograph calibrating reactions.

Reactions	Excitation of residual nucleus (MeV ± keV)	Q value Q_0+E_{ex} (MeV ± keV)
$^{12}C(p,p')^{12}C^*$	4.4398 ± 0.3 [a]	−4.4398 ± 0.3
$^{16}O(p,p')^{16}O^*$	6.1305 ± 0.4 [b]	−6.1305 ± 0.4
$^{16}O(p,d)^{15}O$	0.0	−13.4434 ± 1.2 [c]
$^{27}Al(p,d)^{26}Al$	0.0	−10.8322 ± 2.9 [c]
$^{7}Li(p,d)^{6}Li$	0.0	−5.0280 ± 1.6 [c]
$^{7}Li(p,d)^{6}Li^*$	2.184 ± 2.0	−7.212 ± 3.0 [d]
$^{12}C(^3He,{}^3He')^{12}C^*$	4.4398 ± 0.3	−4.4398 ± 0.3
$^{16}O(^3He,{}^3He')^{16}O^*$	6.1305 ± 0.4	−6.1305 ± 0.4
$^{12}C(^3He,{}^4He)^{11}C$	0.0	1.8582 ± 1.2 [c]
$^{16}O(^3He,{}^4He)^{15}O$	0.0	4.9101 ± 1.3 [c]

[a] C. Chasman, K. W. Jones, R. A. Ristinen, and D. E. Alburger, Phys. Rev. 159, 830 (1967).

[b] J. B. Marion, University of Maryland Technical Report No. ORO-2098-58, 1967 (unpublished).

[c] See Ref. 13.

[d] T. Lauritsen and F. Ajzenberg-Selove, Nucl. Phys. 78, 24 (1966).

The energies of the ^{3}He beams were determined by measuring the rigidities of elastically scattered ^{3}He from ^{12}C and ^{16}O using the calibrated spectrograph. The scattering angle was determined to ±0.03° by measuring the rigidities of ^{3}He from ^{1}H($_3$He, ^{3}He)^{1}H scattering from a Formvar target.

Once the ^{3}He beam energy and scattering angle were determined, more calibration data were taken in the same manner as indicated above. This supplemented the proton calibration data and al-

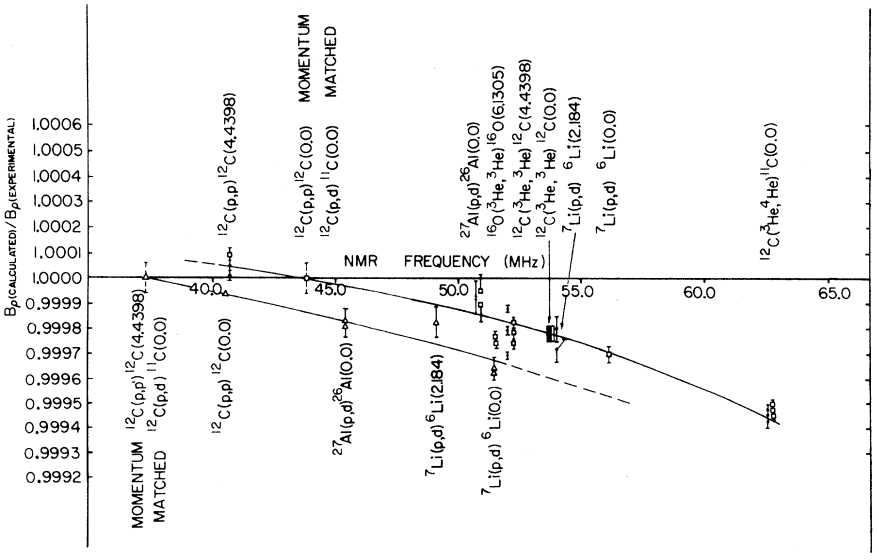

FIG. 1. Calibration of the effective spectrograph field. The calibration is for particles traveling in orbits corresponding to an effective radius of curvature of ~32.3 in. The NMR frequency on the abscissa measures the spectrograph field in a flat field region and the ordinate gives the correction factor for obtaining the correct field.

lowed the calibration to be extended to spectrograph-field strengths of 14.7 kG. Table I lists all the calibration reactions used.

Figure 1 shows the calibration curve obtained from these data. The ordinate is the ratio of the calculated magnetic rigidities [$B\rho$ (calculated)] to the rigidities determined from the product of the NMR field value and the standard radius of curvature [$B\rho$ (experimental)]. This ratio is then plotted against the NMR frequency. The lower curve represents the same sort of calibration using a momentum match of different reactions and normalized at a different field value. As expected, the two curves are approximately parallel.

Since the detector holding apparatus must be moved to compensate for the kinematic energy spread of the various reaction products, this motion was controlled in such a way that the standard position on the focal plane moved along the defined particle orbits.

To preserve the independence of data from one run to another, each ^{3}He run was preceded by its own proton calibration run. Three such runs were made. In addition, within each run, calibration data (including elastic ^{3}He scattering) and ^{6}He data were taken on each of several cycles of the spectrograph magnetic field. The elastic ^{3}He data monitored any changes in beam energy between cycles. Several different carbon and SiO targets were used for the ^{9}C and ^{13}O measurements.

TABLE II. Targets used for (^{3}He, ^{6}He) reactions for E(beam) = 68.0 MeV.

Targets	Thickness (mg/cm^2)	ΔE(^{6}He), average loss (keV)
^{12}C No. 1	0.153	25 ± 3
SiO, F-80	0.227	34 ± 4
"Glass" SiO_2	0.491	71 ± 8
^{24}Mg foil	0.656	83 ± 13
SiO + C	0.432	66 ± 7
^{12}C "F"	0.117	19 ± 3

IV. CALIBRATION UNCERTAINTIES

Uncertainty in the spectrograph calibration curve (Fig. 1) is the consequence of two separate phenomena; the uncertainty in the Q values of reactions used for momentum match, as discussed previously, and the uncertainty in the fit of the calibration curve to the calibrating reactions.

An error in a momentum-match Q value would translate the curve, with only a small change in its shape or tilt. Such a translation of the calibration curve would introduce an error in the calculation of the ^{3}He beam and ^{6}He energies. An error of +1.1 keV in the ^{12}C(p, d)^{11}C Q value would yield an error of +4.7 keV in the beam energy and +2.5 keV in the ^{6}He energies for a ^{3}He beam energy of 68.5 MeV. Since the (^{3}He, ^{6}He) Q value is essentially the difference between the ^{3}He and ^{6}He energies, the error in the Q value is the difference

TABLE III. Experimentally determined (^{3}He, ^{6}He) Q values.

Run number	Reaction	Q value (MeV)	Total error (MeV)	Partial error (MeV)	^{3}He beam energy (MeV)	θ_L (deg)	Target
1-121	^{12}C(^{3}He, ^{6}He)^{9}C	−31.566	±0.020	±0.018	68.574 ± 0.010	14.82	^{12}C No. 1
1-123	^{16}O(^{3}He, ^{6}He)^{13}O	−30.510	±0.020	±0.018	68.577 ± 0.010	14.82	"Glass"
2-89	^{12}C(^{3}He, ^{6}He)^{9}C	−31.574	±0.011	±0.010	68.476 ± 0.008	10.96	^{12}C No. 1
2-89	^{12}C(^{3}He, ^{6}He)^{9}C	−31.581	±0.011	±0.010	68.470 ± 0.008	10.96	^{12}C No. 1
2-106	^{12}C(^{3}He, ^{6}He)^{9}C	−31.597	±0.011	±0.010	68.470 ± 0.008	10.96	^{12}C No. 1
2-93	^{16}O(^{3}He, ^{6}He)^{13}O	−30.506	±0.012	±0.011	68.476 ± 0.008	10.96	SiO, F-80
2-101	^{16}O(^{3}He, ^{6}He)^{13}O	−30.524	±0.012	±0.010	68.470 ± 0.008	10.96	SiO, F-80
2-107	^{16}O(^{3}He, ^{6}He)^{13}O	−30.504	±0.011	±0.010	68.470 ± 0.008	10.96	SiO, F-80
2-103	^{24}Mg(^{3}He, ^{6}He)^{21}Mg	−27.523	±0.018	±0.013	68.470 ± 0.008	10.96	^{24}Mg foil
2-108	^{24}Mg(^{3}He, ^{6}He)^{21}Mg	−27.519	±0.017	±0.010	68.470 ± 0.008	10.96	^{24}Mg foil
3-15	^{12}C(^{3}He, ^{6}He)^{9}C	−31.574	±0.011	±0.010	68.512 ± 0.008	11.01	^{12}C No. 1
3-27	^{12}C(^{3}He, ^{6}He)^{9}C	−31.577	±0.011	±0.009	68.512 ± 0.008	11.01	^{12}C No. 1
3-17	^{16}O(^{3}He, ^{6}He)^{13}O	−30.500	±0.011	±0.010	68.512 ± 0.008	11.01	SiO, F-80
3-28	^{16}O(^{3}He, ^{6}He)^{13}O	−30.514	±0.022	±0.012	68.512 ± 0.008	11.01	"Glass"
3-21	^{24}Mg(^{3}He, ^{6}He)^{21}Mg	−27.499	±0.016	±0.009	68.512 ± 0.008	11.01	^{24}Mg foil
3-29	^{24}Mg(^{3}He, ^{6}He)^{21}Mg	−27.505	±0.017	±0.011	68.210 ± 0.010	11.01	^{24}Mg foil
3-88	^{12}C(^{3}He, ^{6}He)^{9}C	−31.572	±0.012	±0.011	68.210 ± 0.010	10.68	^{12}C "F"
3-77	^{12}C(^{3}He, ^{6}He)^{9}C	−31.572	±0.013	±0.012	68.199 ± 0.010	10.68	^{12}C "F"
3-78	^{16}O(^{3}He, ^{6}He)^{13}O	−30.478	±0.014	±0.011	68.199 ± 0.010	10.68	SiO + C
3-89	^{16}O(^{3}He, ^{6}He)^{13}O	−30.510	±0.014	±0.011	68.210 ± 0.010	10.68	SiO + C
3-90	^{16}O(^{3}He, ^{6}He)^{13}O	−30.510	±0.014	±0.011	68.230 ± 0.010	10.67	SiO + C

of their errors, i.e., +2.2 keV. Similarly, if the error in the (p,d) Q value were −1.1 keV, then the error in the (^{3}He, ^{6}He) Q value would be −2.2 keV.

Using the quoted uncertainties of the calibration reaction Q values, and considering the consistency of the curve shape over several sets of experimental measurements, it is estimated that the uncertainty associated with the fit of the calibration curve, particularly over the region where ^{3}He elastic scattering and ^{6}He were detected, is not greater than $\pm 0.5\times 10^{-4}$ of the outgoing particle energy. This uncertainty was applied directly to the outgoing ^{6}He energies and hence to the calculated Q value. Quantitatively it amounted to about ±2 keV for ^{6}He energies of approximately 36 MeV.

The systematic uncertainties associated with the absolute measurement of the ^{3}He beam energies are so much a function of the calibration procedure and scattering-angle determination, that the values used for ^{3}He beams are effectively defined by these procedures. Systematic errors in its value have therefore been absorbed into these other uncertainties.

Estimates of the beam-energy fluctuations during a run were obtained from the scatter of the ^{3}He calibration reaction points over the course of the run. For example, nine individual measurements of the ^{12}C(^{3}He, ^{3}He)^{12}C elastic peak over the course of a 2-day run varied by a maximum of only 9 keV, with the other calibration reactions showing similar scatter commensurate with their sensitivity to beam energy. This remarkable stability of beam energy was of prime importance to the experiment. The largest such fluctuation for any of the runs was ΔE(beam) = 10 keV.

Fluctuations in the scattering angle caused by possible fluctuation in beam direction during a run was estimated to be no greater than ±0.03°. Since this is reflected in the outgoing ^{6}He energy through the kinematics for each reaction, this effect caused uncertainties in the Q values of ±4.5, ±3.3, and ±2.1 keV in the ^{9}C, ^{13}O, and ^{21}Mg measurements, respectively.

V. TARGETS

The ^{3}He and ^{6}He energy loss in the targets used in this experiment represent a significant correction to the measured ^{6}He energies, and therefore careful measurement of all targets were made. The air-equivalent thicknesses of the targets were measured with an α-source gauge, and the energy losses for various particles were calculated using published tables.[14] The specific ionization of the ^{6}He was taken to be that of a ^{3}He particle at half the ^{6}He energy. Several measurements were made over the surface of each target foil. Since target thickness is measured relative to an equivalent amount of air, precise knowledge of the α energy used is not critical if the stopping power of the target elements are commensurate with that of air. The average energy loss for the outgoing particles in the target was then introduced as an effective excitation energy in the corresponding reaction-kinematics calculations.

The uncertainty in the energy losses was estimated by making several separate measurements of each target and checking their consistency. Table II lists all targets used for this experiment, their air-equivalent thickness, the average energy loss of the ^{6}He particle, and the estimated uncertainty in the energy loss.

For the ^{24}Mg(^{3}He, ^{6}He)^{21}Mg reaction one target was used for all measurements, and energy-loss uncertainty is treated as systematic and applied to the average of the Q-value measurements. For the ^{9}C and ^{13}O measurements several targets were used, and the uncertainties were applied to the Q-value measurements for the corresponding targets.

VI. DATA ANALYSIS

Each Q-value determination was assigned an uncertainty consisting of all relevant parameter fluctuations summed in quadrature. For a particular measurement this included beam-energy fluctuation, scattering-angle fluctuations, statistical error of the peak centroid, uncertainties due to detector nonlinearities for peak centroids not falling exactly at the standard focal-plane position, and any observed magnetic field fluctuations. A weighted average of the measurements for a reaction was then taken using these uncertainties. The systematic uncertainties such as those assigned to the calibration procedure and added to the uncertainty of the average Q value.

The standard deviation of the distribution of in-

TABLE IV. Average Q values and mass excesses for the $T_z = -\frac{3}{2}$ nuclei.

Element	Reaction	Q value (MeV)	Mass excess (MeV)
^{9}C	^{12}C(^{3}He, ^{6}He)^{9}C	−31.578 ± 0.008	28.911 ± 0.009
^{13}O	^{16}O(^{3}He, ^{6}He)^{13}O	−30.506 ± 0.013	23.103 ± 0.014
^{21}Mg	^{24}Mg(^{3}He, ^{6}He)^{21}Mg	−27.512 ± 0.018	10.912 ± 0.018

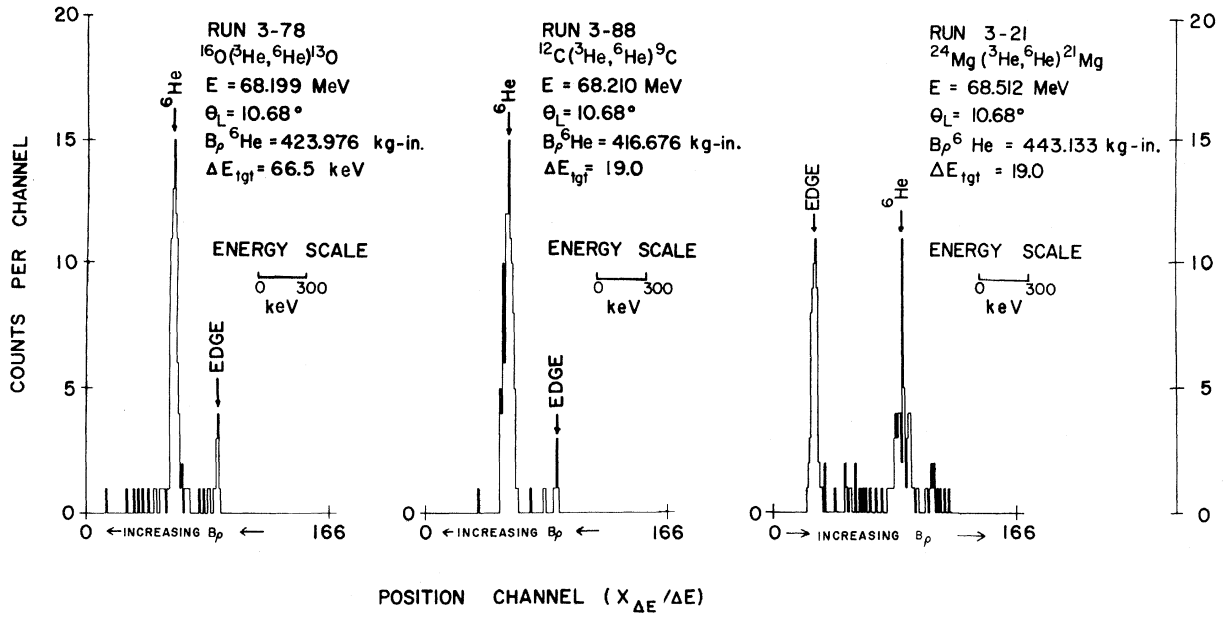

FIG. 2. ^{6}He spectra from position-sensitive detector on spectrograph focal plane.

dividual measurements was also computed for each reaction. In each case the standard deviation of the distribution and the total experimental uncertainty described previously were nearly equal.

In computing the mass excesses of ^{9}C, ^{13}O, and ^{21}Mg, the uncertainties of the other masses involved, ^{3}He, ^{6}He, ^{12}C, ^{16}O, and ^{24}Mg, were also summed with the Q-value uncertainty in quadrature. The uncertainty of ±4.0 keV associated with the ^{6}He mass excess was not negligible in computing the total error of ^{9}C and ^{13}O. The masses of ^{3}He, ^{6}He, ^{12}C, ^{16}O, and ^{24}Mg were taken from Ref. 13.

VII. EXPERIMENTAL RESULTS

Table III lists all individual measurements of the Q values obtained along with the experimental parameters pertinent to each. The column labeled "total error" represents all known experimental uncertainties for that run summed in quadrature as though that were the only measurement made. The column labeled "partial error" represents random errors associated with that particular run, excluding systematic errors that are applied later to the average of the Q values. In Table IV, the resulting average Q values, their uncertainties, and the resulting values for the mass excesses of ^{9}C, ^{13}O, and ^{21}Mg are given.

Figure 2 displays typical position spectra for the the (^{3}He, ^{6}He) reactions where the abscissa is the position signal (XE/E). Figure 3 shows the angular distribution for the ^{12}C(^{3}He, ^{6}He)^{9}C reaction.

VIII. DISCUSSION

Table V gives the coefficients of the IMME for the $A = 9$, 13, and 21 isobaric quartets. The coefficients $a(\alpha, T)$, $b(\alpha, T)$, and $c(\alpha, T)$ were obtained from a least-squares fit of the form

$$M = a(\alpha, T) + b(\alpha, T)T_z + c(\alpha, T)T_z^2$$

to the mass excesses of the quartet members. The $d(\alpha, T)$ coefficient is the coefficient of a T_z^3

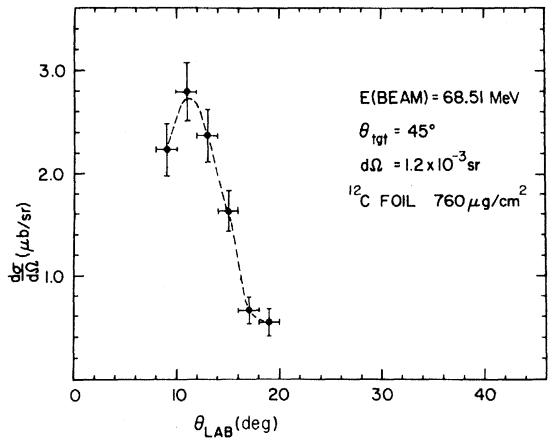

FIG. 3. Angular distribution of ^{6}He for the reaction ^{12}C(^{3}He, ^{6}He)^{9}C. The curve is to guide the eye.

TABLE V. Empirically determined coefficients for the mass equation of the form $M=a(\alpha, T)+b(\alpha, T)T_z+c(\alpha, T)T_z^2$ and $M=a(\alpha, T)+b(\alpha, T)T_z+c(\alpha, T)T_z^2+d(\alpha, T)T_z^3$ using the $T_z=-\frac{3}{2}$ mass excess values of the present work. (For mass excesses of $T_z=\frac{3}{2}$, $\pm\frac{1}{2}$; for $T=\frac{3}{2}$ multiplet members see Table I in Ref. 2) The coefficients were determined from a weighted least-squares fit, and the χ^2 of the quadratic fit is indicated.

Mass	$a(\alpha, T)$	$b(\alpha, T)$	$c(\alpha, T)$	$d(\alpha, T)$	χ^2
9	26.343±0.004	−1.319±0.003	0.266±0.003	···	4.0
13	19.257±0.003	−2.180±0.004	0.256±0.003	···	0.002
21	4.899±0.005	−3.657±0.005	0.240±0.005	···	1.28
9	26.343±0.004	−1.334±0.008	0.265±0.003	0.008 ±0.004	···
13	19.257±0.003	−2.180±0.005	0.256±0.004	0.0002±0.0035	···
21	4.899±0.005	−3.665±0.009	0.238±0.005	0.0057±0.0051	···

term when the same data are fit to the expression

$$M=a(\alpha, T)+b(\alpha, T)T_z+c(\alpha, T)T_z^2+d(\alpha, T)T_z^3.$$

For both cases the mass-excess values for the $T=\pm\frac{1}{2}$, $+\frac{3}{2}$ members are taken from Table 1 of Ref. 2. The term χ^2 represents the quality of the fit where

$$\chi^2=\sum\left[\frac{m(\text{calc})-m(\text{exp})}{m(\text{exp})}\right]^2.$$

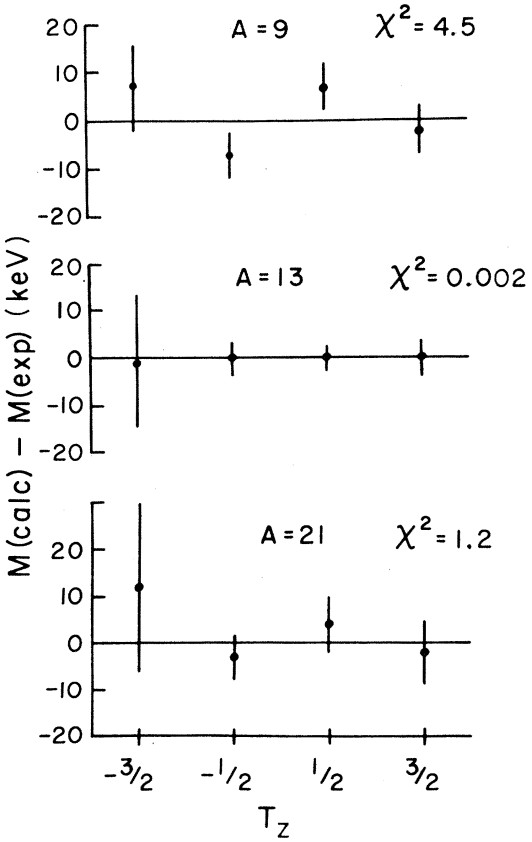

FIG. 4. Deviation of experimental $T=\frac{3}{2}$ multiplet members from the quadratic mass equation using the coefficients of Table V. The $T_z=-\frac{3}{2}$ members are from the present work, the $T_z=+\frac{3}{2}$, $\pm\frac{1}{2}$ members from Ref. 2.

Deviations of the experimentally determined masses and predictions of the IMME with the a, b, and c coefficients of Table V are displayed graphically in Fig. 4. Only the $A=9$ quartet shows deviations greater than the experimental uncertainty of the points.

The addition of higher-order terms such as T_z^3 and T_z^4 to the IMME are predicted if the nuclear forces are charge dependent or when the Coulomb potential is expanded as a second-order perturbation. Such a second-order perturbation can be treated in various ways. In Table VI,[15-17] various calculated values of the d coefficient are shown in comparison with the empirical values determined here.

Janecke[15] has used a second-order treatment that involves mixing of the $T_z=\pm\frac{1}{2}$ members of the quartet with nearby states of the lower T. In this case the IMME is expanded to the fourth power of T_z and predicts that terms in T_z^3 and T_z^4 will be small, not so much because the perturbation is small, but because the major effects of such perturbations are absorbed mostly in the T_z and T_z^2 terms. The calculated d coefficients are shown in the third column in Table VI.

Another attempt to make some estimate of the size of the cubic term is presented by Henley and Lacy,[16] where the Schrödinger equation is solved directly for a nuclear model. The model consists of three nucleons outside an inert core, with each of these extra nucleons in a Woods-Saxon nuclear potential, a Lane symmetry potential, and the Coulomb potential of a uniformly charged sphere with radius equal to that of the Woods-Saxon well. The coefficients for the T_z and T_z^2 terms agree with experimental values, generally to within 10–20%. The predicted d coefficient is shown in the fourth column in Table VI.

Bertsch and Kahana[17] have calculated the coefficient of the cubic terms by considering just the specific second-order perturbation in the Coulomb interaction between protons. They also treated the $T=\frac{3}{2}$ multiplet as three valence nucleons outside of an inert core, and used Woods-Saxon wave

TABLE VI. Comparison of experimental and theoretical values of the coefficient of a cubic term in the IMME.

Mass	Exp. value (keV)	Janecke [a] (keV)	Henley and Lacy [b] (keV)	Bertsch and Kahana [c] (keV)	$Z\alpha c$ [b] (keV)
9	8.3±3.9	5.8±4.2	0.064 65	1.6	9.0
13	−0.2±3.5	···	−0.439 90	0.9	12.0
21	5.7±5.1	···	−0.181 68	0.3	19.0

[a]See Ref. 15. [b]See Ref. 16. [c]See Ref. 17.

functions and a purely Coulomb force. Their values are shown in the fifth column in Table VI.

Also it has been estimated[2,5,18] that the size of the d coefficient may be $\simeq Z\alpha c$ where Z is the average charge of the multiplet, α is the fine-structure constant, and c the coefficient of T_z^2. For the $A=9$ quartet this would be $\simeq 9$ keV, and the data indicate a d term of this magnitude.

If we consider the Coulomb energy of a uniformly charged spherical nucleus, i.e., $3Z(Z-1)e^2/5R_0A^{1/3}$, the term $Z(Z-1)$ may be expanded in terms of T_z and T_z^2 with resulting IMME coefficients[2]:

$$b=-0.6(A-1)e^2/R_0A^{1/3}+(M_n-M_p),$$

$$c=0.6e^2/R_0A^{1/3},$$

where M_n-M_p is the neutron-proton mass difference. The radius parameter T_0 can then be calculated from the empirically determined b and c, and the results are shown in Fig. 5, where $R_0(b)$ and $R_0(c)$ are extracted for the b and c coefficients, respectively. They should have the same value for a given A if the mass difference other than the proton-neutron mass difference between the members of the multiplet is attributable to the difference in the electrostatic energy of a uniform charge distribution. As can be seen in Fig. 5,[19] the b and c coefficients yield quite different results for some of the nuclei. This may reflect the effect of the contribution of individual protons to the total Coulomb energy as determined by the detail of their nuclear wave function.[20]

The IMME appears to be a rather insensitive probe of particular charge-dependent phenomena. As discussed in detail by Janecke,[15] Garvey,[2] and by Wilkinson,[18] the fact that very good IMME fits to the data of isobaric quartets may be obtained does not necessarily mean that the assumptions from which it may be derived are necessarily true. The reason for this lies in the fact that the quadratic nature of the equation enables it to ab-

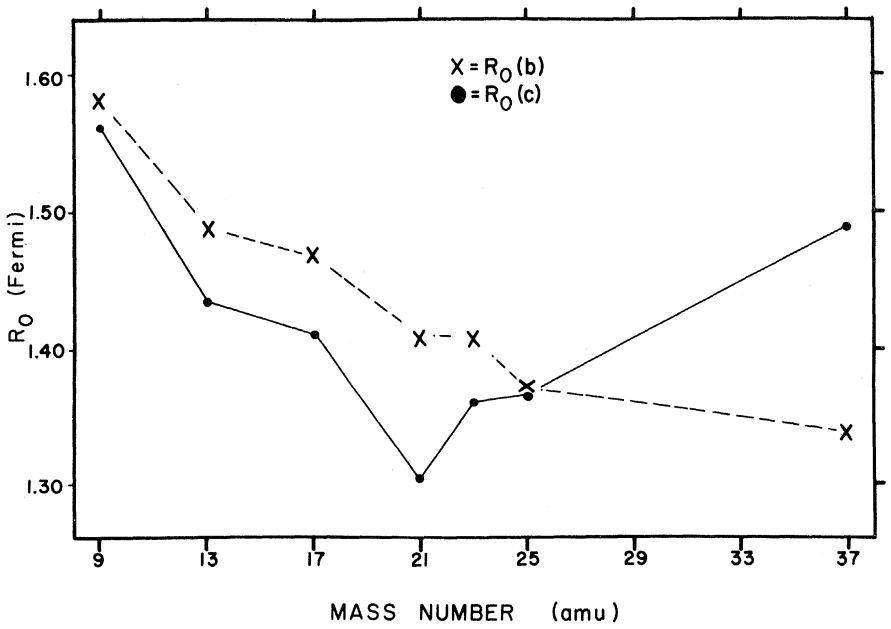

FIG. 5. Radius parameters as derived from the most recent determination of the b and c coefficients in the IMME. The Coulomb contribution to the mass difference between multiplet members is assumed to arise from a uniform spherical charge distribution of radius $R_0A^{1/3}$. Mass-equation coefficients b and c for $A=9$, 13, 21 are from the present work; for $A=17$, 25, 37 from Table I of Ref. 19; and for $A=23$ from Table II, Ref. 2.

sorb many other phenomena as perturbations with accuracy sufficient to fit existing data well.

Even more accurate determination of the masses remains a worthwhile goal. The experimental procedures developed in this work allow one to make high-precision absolute Q-value measurements even at high bombarding energies and thus makes possible the study of proton-rich nuclei that have been inaccessible by other techniques.

ACKNOWLEDGMENTS

We would like to thank the Michigan State University cyclotron laboratory staff for their continued support throughout this experiment.

---

*Work supported by the National Science Foundation.

†Present address: Physics Department, University of South Carolina, Columbia, South Carolina.

[1]E. P. Wigner, in *Proceedings of the Robert A. Welch Foundation Conference on Chemical Research,* edited by W. O. Milligan (Robert A. Welch Foundation, Houston, Texas, 1957), p. 67.

[2]G. T. Garvey, in *Proceedings of the Second Conference on Nuclear Isospin, Asilomar-Pacific Grove, California, 13–15 March 1969,* edited by J. D. Anderson, S. D. Bloom, J. Cerny, and W. W. True (Academic Press Inc., New York, 1969), p. 703.

[3]C. A. Barnes, E. G. Adelberger, D. C. Hensley, and A. B. McDonald, in *Nuclear Physics: An International Conference,* edited by R. L. Becker, C. D. Goodman, P. H. Stelson, and A. Zucker (Academic Press Inc., New York, 1967), p. 261.

[4]J. M. Mosher, R. W. Kavanagh, and T. A. Tombrello, Bull. Am. Phys. Soc. 14, 1167 (1969).

[5]J. Cerny, Ann. Rev. Nucl. Sci. 18, 27 (1968).

[6]G. F. Trentelman, B. M. Preedom, and E. Kashy, Phys. Rev. Letters 25, 530 (1970).

[7]J. E. Spencer and H. A. Enge, Nucl. Instr. Methods 49, 181 (1967).

[8]G. H. Mackenzie, E. Kashy, M. M. Gordon, and H. G. Blosser, IEEE Trans. Nucl. Sci. 14, 450 (1967).

[9]R. K. Jolly, G. F. Trentelman, and E. Kashy, Nucl. Instr. Methods 87, 325 (1970).

[10]D. Bayer, TOOTSIE XDS Sigma-7 Computer Assembly Language Code for On-Line Data Acquisition, Michigan State University Cyclotron Laboratory Internal Report, 1970 (unpublished).

[11]J. L. Snelgrove and E. Kashy, Nucl. Instr. Methods 52, 153 (1967).

[12]G. F. Trentelman and E. Kashy, Nucl. Instr. Methods 82, 304 (1970).

[13]C. Maples, G. W. Goth, and J. Cerny, University of California Radiation Laboratory Report No. UCRL-16964, 1966 (unpublished).

[14]C. F. Williamson, J. P. Bouyot, and J. Picard, Centre d'Etudes Nucléaires de Saclay, France Report No. CEA-R3042, 1966 (unpublished).

[15]J. Janecke, Nucl. Phys. A128, 632 (1969).

[16]E. M. Henley and C. E. Lacy, Phys. Rev. 184, 1228 (1969).

[17]G. Bertsch and S. Kahana, Phys. Letters 33B, 193 (1970).

[18]D. H. Wilkinson, Phys. Rev. Letters 13, 571 (1964); Phys. Letters 12, 348 (1964).

[19]R. Mendelson, G. J. Wozniak, A. D. Bacher, J. M. Losieaux, and J. Cerny, Phys. Rev. Letters 25, 533 (1970).

[20]J. A. Nolen, Jr., and J. P. Schiffer, Ann. Rev. Nucl. Sci. 19, 471 (1969).